VII International Conference on Computational Methods for Coupled Problems in Science and Engineering
COUPLED PROBLEMS 2017
M. Papadrakakis, E. Oñate and B. Schrefler (Eds)

A NEW MATERIAL DESCRIPTION FOR PLANT TISSUES UNDER FROST EXPOSURE

Lukas Eurich*, Arndt Wagner* and Wolfgang Ehlers*

*Institute of Applied Mechanics
University of Stuttgart
Pfaffenwaldring 7, D-70569 Stuttgart, Germany
e-mail: Lukas.Eurich@mechbau.uni-stuttgart.de, www.mechbau.uni-stuttgart.de/ls2

Key words: Plant freezing, thermoelasticity, strain energy, compaction point, Theory of Porous Media

Abstract. Plant tissues exhibit a cellular structure, where the tissue cells compose a solid skeleton, and the intercellular space is filled with gaseous air and/or liquid water. Under frost exposure, the pore water may freeze and turn into solid ice. As a multiphasic material, plant tissues can be meaningfully described by the Theory of Porous Media (TPM). In the proposed TPM approach, the solid constituents, i. e. the solid skeleton and the ice, are kinematically coupled and described within the framework of thermoelasticity. Generally, porous media with assumed materially incompressible solid constituents are described as a compressible material, since a volumetric deformation can be realised by a volume change of the pore space. However, freezing of the pore water leads to an increase of the solidity even until a vanishing of the pore space. Therefore, the so-called point of compaction (compression until the pore space is cleared) needs to be considered in the material description of the solids. The present contribution aims to introduce a quarternary modelling approach applied to frost-resistant plant tissues with an emphasis on the description of coupled thermoelastic effects. In particular, the impact of pore-water freezing on the derivation of a strain-energy function for plant tissues is discussed leading to a new thermodynamically consistent material formulation.

1 INTRODUCTION

Frost-resistant plants have developed several strategies to cope with subzero temperatures. For example, plants have developed strategies to hinder freezing, e. g. by deep supercooling [1], which is a phenomenon describing a significant lowering of the ice nucleation temperature, way below $0°C$. But they have also developed strategies when ice formation cannot be prevented. In that case, the porous structure of plants plays a crucial role. The porous structure is originated by the arrangements of single cells [2]. Therefore,

the tissue cells are considered as the solid skeleton, while the intercellular space is filled with gaseous air and liquid water. The crucial mechanism, when freezing cannot be prevented, is the dehydration of the cell body [2], since freezing within the cells represents a critical process threatening the ability of a plant to survive [3]. This mechanism, where the water is with decreasing temperature no longer trapped within the cell body, leads to a change in solidity. Therefore, the water loss of the cell body represents one type of mass transfer. Another type of mass transfer occurs within the pore space, i. e. the phase change of the water from a liquid state of aggregation to a solid one. This also leads to a change in solidity. Due to the assumed material incompressibility of the solid components, one has to consider the compaction point when the overall behaviour changes its characteristic from compressible to incompressible as the pore space vanishes. This was described by Ehlers & Eipper [4] for materials under isothermal conditions by introducing an additive split of the strain-energy function of a *Simo-Pister*-type material description, where the necessary condition of the compaction point was included. Bluhm [5] extended this approach to non-isothermal conditions, however, with the assumption of constant effective densities and no inclusion of mass transfer. Based on these works, a material description is needed for plant tissues, which can be modelled as thermoelastic porous materials, characterised by two solid (materially incompressible) components including mass transfer and the existence of the compaction point.

2 MODELLING FROST-RESISTANT PLANT TISSUES

2.1 Quarternary modelling approach

Since plants are porous materials, a sound multicomponent and multiphasic model is realised within the TPM. Its current understanding is outlined in the fundamental works of de Boer [6] and Ehlers [7, 8] and citations therein. Relevant approaches with regard to phase transition processes within the TPM are given in Ehlers & Häberle [9] and Bluhm et al. [10].

Applying the TPM to frost-resistant plant tissues, the basic model consists of four constituents φ^α, cf. to Eurich et al. [11], namely tissue cells ($\alpha = S$), which contain initially trapped water, a pore gas ($\alpha = G$) and pore water ($\alpha = L$), which may turn into ice ($\alpha = I$), such that

$$\varphi = \bigcup_\alpha \varphi^\alpha = \varphi^S + \varphi^G + \varphi^L + \varphi^I. \tag{1}$$

As a basic prerequisite of the TPM, these constituents are volumetrically averaged over a representative elementary volume (REV). This results in a homogenised continuum-mechanical model with superimposed and mutually interacting constituents, as shown in Figure 1. The local amount of each constituent φ^α can be addressed by the volume fraction

$$n^\alpha = \frac{\mathrm{d}v^\alpha}{\mathrm{d}v}. \tag{2}$$

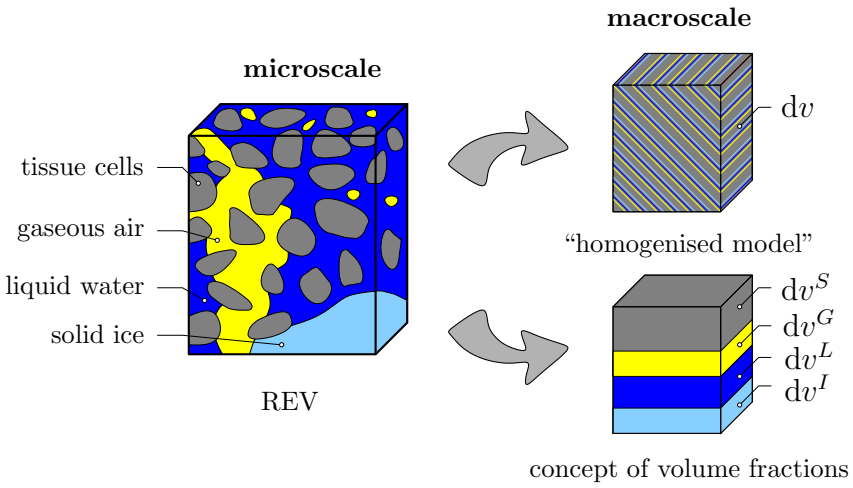

Figure 1: Representative elementary volume (REV) with schematically displayed microstructure of frost-resistant plant tissues and macroscopic multiphasic and multicomponent modelling approach.

Since there is no empty space in the domain, the volumetric constraint

$$\sum_{\alpha} n^{\alpha} = n^{S} + n^{G} + n^{L} + n^{I} = 1 \tag{3}$$

holds. Having the definition of the local volume fraction in mind, two densities can be introduced, the effective (realistic) density $\rho^{\alpha R} = \mathrm{d}m^{\alpha}/\mathrm{d}v^{\alpha}$ as the ratio between the mass element $\mathrm{d}m^{\alpha}$ of a constituent φ^{α} and its volume element $\mathrm{d}v^{\alpha}$ and the partial density $\rho^{\alpha} = \mathrm{d}m^{\alpha}/\mathrm{d}v$ as the ratio between the mass element $\mathrm{d}m^{\alpha}$ and the volume element $\mathrm{d}v$ of the overall aggregate. These two measures are connected by the volume fraction via $\rho^{\alpha} = n^{\alpha}\rho^{\alpha R}$. For materially incompressible constituents (such as in the present model the solid skeleton, the ice and the water), the realistic density depends only on temperature. Instead, the realistic density of materially compressible materials (such as air) is a function of temperature and pressure.

2.2 Kinematics

2.2.1 State of motion and kinematic coupling of the solid constituents

Within the framework of the TPM, each constituent φ^{α} can, in general, have an independent state of motion. In order to guarantee independent motion functions, one has to introduce formally individual motion functions and velocities for each constituent, viz.:

$$\mathbf{x} = \boldsymbol{\chi}_{\alpha}(\mathbf{X}_{\alpha}, t), \quad \overset{\prime}{\mathbf{x}}_{\alpha} = \frac{\partial}{\partial t}\boldsymbol{\chi}_{\alpha}(\mathbf{X}_{\alpha}, t). \tag{4}$$

Therein, the motions and velocities depend on the reference configuration $\mathbf{X}_\alpha$ of the respective constituents. The deformation of the solid skeleton is described by the material deformation gradient

$$\mathbf{F}_S = \frac{\partial \boldsymbol{\chi}_S(\mathbf{X}_S, t)}{\partial \mathbf{X}_S}. \tag{5}$$

For the motion of the ice, a kinematic coupling is introduced as sketched in Figure 2. Therefore, the ice is assumed to be attached to the solid skeleton when the pore water is freezing [10]. This implies that drifting ice particles in the pore space are not considered.

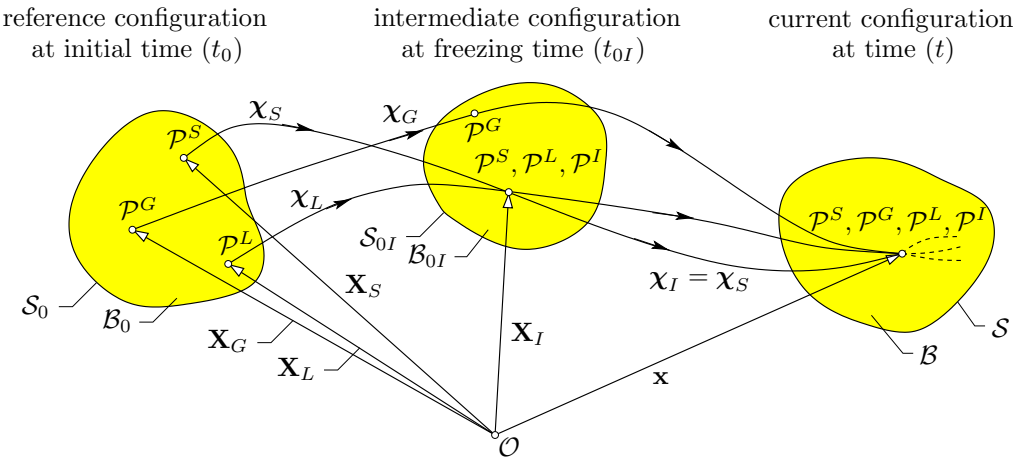

Figure 2: State of motion and kinematic coupling of the quarternary TPM model.

With this kinematic coupling, the motion of the solid skeleton and the ice is divided into a state before the ice formation is initiated, i. e. the pore water is liquid, and a state thereafter. Before freezing, the liquid pore water can be mobile within the pore space. The intermediate configuration represents the reference configuration $\mathbf{X}_I$ where the liquid water turns into solid ice and is attached to the solid skeleton. Therefore, the motion of the solid skeleton and the ice for subsequent configurations is kinematically coupled, indicating an identical state of motion and identical velocities via

$$\boldsymbol{\chi}_I(\mathbf{X}_I, t) = \boldsymbol{\chi}_S(\mathbf{X}_S, t), \quad \Rightarrow \quad \overset{\prime}{\mathbf{x}}_I = \overset{\prime}{\mathbf{x}}_S. \tag{6}$$

In order to define the deformation gradient of the ice, we proceed from the respective derivatives

$$\frac{\partial \boldsymbol{\chi}_S(\mathbf{X}_S, t)}{\partial \mathbf{X}_S} = \frac{\partial \boldsymbol{\chi}_I(\mathbf{X}_I, t)}{\partial \mathbf{X}_S} = \frac{\partial \boldsymbol{\chi}_I(\mathbf{X}_I, t)}{\partial \mathbf{X}_I} \frac{\partial \mathbf{X}_I}{\partial \mathbf{X}_S}. \tag{7}$$

With the definition of the material deformation gradient for the solid skeleton (5), the expression above can be used to formulate the material deformation gradient of the ice according to (7), viz.

$$\mathbf{F}_S \;=\; \mathbf{F}_I \mathbf{F}_{S0} \quad \Rightarrow \quad \mathbf{F}_I \;=\; \mathbf{F}_S \mathbf{F}_{S0}^{-1}. \tag{8}$$

This implies that the deformation gradient of the solid skeleton can be split multiplicatively into the deformation $\mathbf{F}_{S0}$ before the onset of the phase transition and a deformation $\mathbf{F}_I$ after the onset. The volumetric deformation of the solid skeleton and the ice can be derived based on the determinants of $\mathbf{F}_S$ and $\mathbf{F}_I$, via

$$\begin{aligned} J_S \;&=\; \det \mathbf{F}_S \\ J_I \;&=\; \det \mathbf{F}_I \;=\; \det \left(\mathbf{F}_S \, \mathbf{F}_{S0}^{-1}\right) \;=\; \det \mathbf{F}_S \det \mathbf{F}_{S0}^{-1} \;=\; J_S / J_{S0}. \end{aligned} \tag{9}$$

2.2.2 Decomposition of the thermoelastic deformation

The inclusion of thermal effects into the coupled description of deformation for thermoelastic materials can be achieved by a multiplicative split of the deformation gradient $\mathbf{F}_\delta$ for the solid constituents $\delta = \{S, I\}$, cf. [12]. Here, the approach of Lu & Pister [13] is used

$$\mathbf{F}_\delta \;=\; \frac{\partial \boldsymbol{\chi}_\delta(\mathbf{X}_\delta, t)}{\partial \mathbf{X}_\delta} \;=\; \mathbf{F}_{\delta M} \mathbf{F}_{\delta\theta}, \tag{10}$$

where $\mathbf{F}_{\delta M}$ represents the purely mechanical part of the deformation and $\mathbf{F}_{\delta\theta}$ the purely thermal part, which is defined by a fictive mechanical unloading.

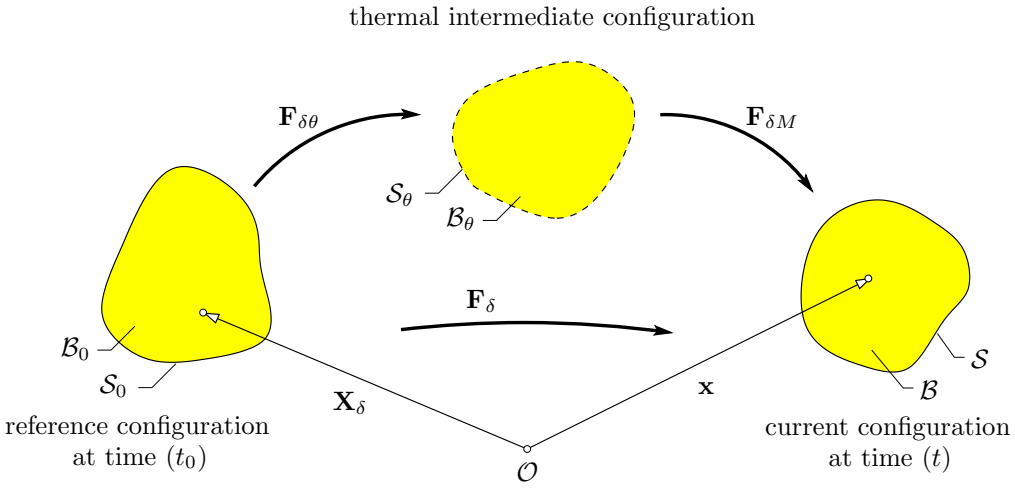

Figure 3: Multiplicative decomposition of the thermoelastic deformation.

Since isotropic thermally induced volume changes are assumed, the thermal deformation is, according to [13], given via

$$\mathbf{F}_{\delta\theta} = (\det \mathbf{F}_{\delta\theta})^{1/3}\,\mathbf{I}, \quad \det \mathbf{F}_{\delta\theta} = \exp\left[3\alpha^{\delta}(\theta - \theta^{\delta}_{0\delta})\right]. \tag{11}$$

2.3 Volume fractions

An energetic inclusion of the compaction point into the material description requires the specification of the volume fractions of the respective solid constituents. These can be derived by evaluating mass balances of the constituents

$$(\rho^{\alpha})'_{\alpha} + \rho^{\alpha}\operatorname{div}\overset{\prime}{\mathbf{x}}_{\alpha} = \hat{\rho}^{\alpha}, \tag{12}$$

where $(\rho^{\alpha})'_{\alpha}$ denotes the material time derivative of the partial density with respect to the motion of φ^{α} and $\hat{\rho}^{\alpha}$ is the mass exchange (in the present case the cell dehydration and the freezing of the pore water). As the material density of the solid skeleton and the ice are due to the material incompressibility solely a function of temperature and given via

$$\rho^{\delta R} = \rho^{\delta R}_{0\delta}(\det \mathbf{F}_{\delta\theta})^{-1} = \rho^{\delta R}_{0\delta} e^{-3\alpha^{\delta}(\theta-\theta^{\delta}_{0\delta})}, \tag{13}$$

the volume fraction can be derived by a formal integration of the mass balances and considering the temperature-dependent density $\rho^{\delta R}$ which results in

$$n^{\delta} = \frac{n^{\delta}_{0\delta}}{\det \mathbf{F}_{\delta M}} \exp\Big(\int_{t_0}^{t} \frac{\hat{\rho}^{\delta}}{\rho^{\delta}}\,\mathrm{d}\tau\Big). \tag{14}$$

This indicates that the volume fraction of the solid skeleton can be decomposed into a growth-dependent part and a part that depends on the mechanical deformation.

3 STRAIN-ENERGY FORMULATION

3.1 Introduction of the compaction point for a thermoelastic solid with mass transfer

For the development of an appropriate material description for the solid skeleton, the material incompressibility needs to be considered. However, due to the porous structure also large volumetric deformations can occur when the porosity changes, which indicates in general $J_S = \det \mathbf{F}_S \neq 1$. Therefore, according to Ehlers & Eipper [4] and Bluhm [5] a compressible material law has to be considered as long as the pore space can be compressed. However, in the present case when ice formation occurs, the pore space vanishes ($n^F = 0$). In accordance, this indicates an incompressible characteristic and, hence, the existence of the compaction point.

As the volume fractions are essential for the development of the strain-energy function, their amount is specified for the respective solid constituents by

$$n^S = \frac{n^S_{0S}\, J_{S\theta}}{J_S} \exp\Big(\int_{t_0}^{t} \frac{\hat{\rho}^S}{\rho^S}\,\mathrm{d}\tau\Big), \quad n^I = \frac{n^I_{0I}\, J_{I\theta}}{J_I} \exp\Big(\int_{t_0}^{t} \frac{\hat{\rho}^I}{\rho^I}\,\mathrm{d}\tau\Big), \tag{15}$$

where $J_{SM} = \det \mathbf{F}_{SM}$, $J_{S\theta} = \det \mathbf{F}_{S\theta}$, $J_{S0} = \det \mathbf{F}_{S0}$, $J_{IM} = \det \mathbf{F}_{IM}$ and $J_{I\theta} = \det \mathbf{F}_{I\theta}$ determine the volumetric deformations. Since the motion of the ice and the solid skeleton is coupled, there exists a relation between the corresponding volumetric deformations according to equation $(9)_2$, which results in

$$\frac{J_{SM}\, J_{S\theta}}{J_{S0}} \;=\; J_{IM}\, J_{I\theta}. \tag{16}$$

At the compaction point, the pore space vanishes indicated by $n^S + n^I = 1$. Considering the integrated volume balances, the volumetric deformation of the solid skeleton is constrained by the compaction point

$$\tilde{J}_S \;=\; n^S_{0S}\, J_{S\theta} \exp\Big(\int_{t_0}^{t} \frac{\hat{\rho}^S}{\rho^S}\, \mathrm{d}\tau\Big) + n^I_{0I} J_{S0}\, J_{I\theta} \exp\Big(\int_{t_0}^{t} \frac{\hat{\rho}^I}{\rho^I}\, \mathrm{d}\tau\Big). \tag{17}$$

Therefore, the constraint for the volumetric deformation of the solid skeleton reads

$$0 < \tilde{J}_S < J_S < \infty. \tag{18}$$

3.2 Additive split of the strain-energy function for the solid skeleton

The basis for the considerations concerning the development of the strain-energy function W^S is a *Simo-Pister*-type material law [14], which was originally proposed for a compressible material under isothermal conditions in the form

$$W^S(I_S, J_S) \;=\; \overline{U^S}(J_S) + w^S(I_S) \;=\; U^S(J_S) - \mu^S \ln J_S + \frac{\mu^S}{2}(I_S - 3), \tag{19}$$

where $I_S = \mathbf{C}_S \cdot \mathbf{I}$ is the first invariant of the right *Cauchy-Green* deformation tensor $\mathbf{C}_S = \mathbf{F}_S^T\, \mathbf{F}_S$. For the specification of $U^S(J_S)$ several approaches, depending on the application, are on the market. Their characteristics are reviewed in Hartmann [15]. For a porous medium under isothermal conditions describing the compaction point, the approach by Ehlers & Eipper [4] is emphasised.

For a thermoelastic material, the above mentioned form of equation (19) can be extended to account for thermal effects [5]

$$\begin{aligned} W^S(\theta, I_S, J_S) \;=& U^S(J_S) - \mu^S \ln J_S + \frac{\mu^S}{2}(I_S - 3) - 3\alpha^S k^S \ln J_S (\theta - \theta^S_{0S}) - \\ & - \rho^S_{0S} c^S \Big(\theta \ln \frac{\theta}{\theta^S_{0S}} - \theta + \theta^S_{0S}\Big), \end{aligned} \tag{20}$$

where μ^S is the second *Lamé* constant, α^S the thermal expansion coefficient, k^S the bulk modulus and c^S the specific heat. The temperature is denoted by θ, whereas θ^S_{0S} is the initial temperature.

3.3 Constraints and a new strain-energy function

Within the framework of the TPM, hyperelastic material descriptions, where the extra stresses can be derived from an energy potential [7], require for the consideration of the compaction point the following conditions to be fulfilled [4].

Undeformed configuration: In the undeformed configuration, i. e. $J_S = 1$, the strain energy as well as the hydrostatic *Cauchy* stress vanishes, viz.:

$$U^S(J_S = 1) \;=\; 0 \quad \text{and} \quad \frac{\partial U^S}{\partial J_S}(J_S = 1) = 0. \tag{21}$$

Compaction point: In the case that the deformation reaches the compaction point, the necessary energy and the hydrostatic compressive stress have to be infinite

$$U^S(J_S \to \tilde{J}_S) \to +\infty \quad \text{and} \quad \frac{\partial U^S}{\partial J_S}(J_S \to \tilde{J}_S) \to -\infty. \tag{22}$$

This condition replaces the condition for non-porous, compressible materials, where the singularity is reached when $J \to 0$. Here, the transition from the compressible to an incompressible material law represents a singularity.

Growth condition: When the local porosity approaches unity, the necessary energy and the necessary (tensile) stress have to be infinite

$$U^S(J_S \to +\infty) \to +\infty \quad \text{and} \quad \frac{\partial U^S}{\partial J_S}(J_S \to +\infty) \to +\infty. \tag{23}$$

Convexity condition: In order to ensure local material stability, polyconvexity of the overall strain energy W^S has to be fulfilled [16]. Under the assumption that the volumetric extension U^S is twice differentiable, this conditions requires the second derivative with respect to the Jacobian J_S to be positive semi-definite

$$\frac{\partial^2 U^S}{\partial J_S^2} \geq 0, \quad \forall J_S > \tilde{J}_S > 0. \tag{24}$$

Compatibility assumption: As the linearised material law is supposed to result in *Hooke*'s law, the first *Lamé* constant Λ^S is determined via

$$\Lambda^S \;:=\; \frac{\partial^2 U^S}{\partial J_S^2}(J_S = 1). \tag{25}$$

A new polyconvex strain energy: An analogous procedure as presented by Ehlers & Eipper [4] leads to a material description in a comparable form that meats the requirement of the present case:

$$\begin{aligned} U^S(J_S) \;=\; \frac{\Lambda^S}{\gamma_0^S(\gamma_0^S - 1) + \frac{2}{(\tilde{J}_S - 1)^2}} \Big[J_S^{\gamma_0^S} - (\gamma_0^S + \frac{2}{\tilde{J}_S - 1}) J_S + \\ + \gamma_0^S + \frac{2}{\tilde{J}_S - 1} - 1 + \ln\big(\frac{(\tilde{J}_S - 1)^2}{(\tilde{J}_S - J_S)^2}\big) \Big]. \end{aligned} \tag{26}$$

Therein, $\gamma_0^S \geq 1$ is a material parameter controlling the volumetric behaviour, cf. [17].

3.4 Discussion of the volumetric extension to the strain-energy function

Within the framework of hyperelasticity, the mechanical extra stress in terms of *Cauchy* stress can be derived based on thermodynamical considerations via

$$\mathbf{T}^S_{E\,mech} = 2\frac{\rho^S}{\rho^S_{0S}}\mathbf{F}_S\frac{\partial W^S}{\partial \mathbf{C}_S}\mathbf{F}_S^T. \tag{27}$$

For a study concerning the compaction point, only the stress originating from the volumetric extension $U^S(J_S)$ under isothermal conditions is considered, viz.

$$\frac{\partial U^S}{\partial J_S} = \frac{\Lambda^S}{\gamma_0^S(\gamma_0^S-1)+\frac{2}{(\tilde{J}_S-1)^2}}\left(\gamma_0^S J_S^{\gamma_0^S-1} - \gamma_0^S - \frac{2}{\tilde{J}_S-1} + \frac{2}{\tilde{J}_S - J_S}\right). \tag{28}$$

Note that for each configuration the limiting value $\tilde{J}_S$ for the Jacobian J_S may change, particularly due to mass transfer. For further discussions $\gamma_0^S = 2$ was chosen. This yields the form for compressible solid constituents under isothermal conditions according to Simo & Taylor [18], as shown in [15], when there is no compaction point, i. e. $\tilde{J}_S = 0$. This exemplary situation is compared to the case with compaction point, where the limiting value $\tilde{J}_S = 0.5$ of the Jacobian was chosen. Figure 4 shows that a deformation state under compression is penalised when getting too close to the point of compaction.

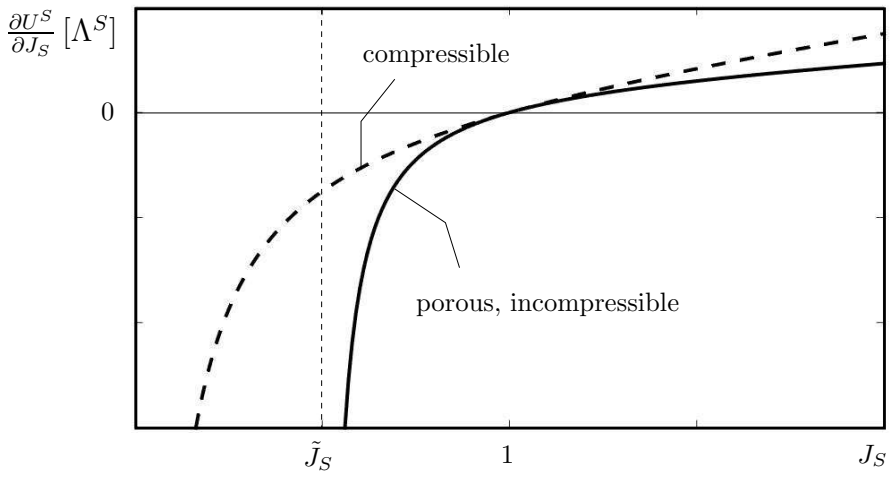

Figure 4: Characterisation of compressible materials and porous, materially incompressible materials with compaction point $\tilde{J}_S$.

Furthermore, the material description has been investigated by a virtual tension-compression test indicating a uniaxial state of stress. Note in passing that stability issues

under compression are not addressed. The deformation is given via

$$\mathbf{F}_S = \begin{bmatrix} \lambda & 0 & 0 \\ 0 & \lambda_L & 0 \\ 0 & 0 & \lambda_L \end{bmatrix} \mathbf{e}_i \otimes \mathbf{e}_j, \quad J_S = \lambda \lambda_L^2, \tag{29}$$

where $\lambda = L/L_0$ is the axial stretch and λ_L the unknown lateral stretch. When isothermal conditions are assumed, the lateral stress according to (27) in the directions $\mathbf{e}_2$ and $\mathbf{e}_3$ vanishes

$$0 = \frac{\nu(\tilde{J}_S - 1)^2}{(1-2\nu)(\tilde{J}_S^2 - 2\tilde{J}_S + 2)} \left[2\lambda\lambda_L^2 - \frac{2\tilde{J}_S}{\tilde{J}_S - 1} + \frac{2}{\tilde{J}_S - (\lambda\lambda_L^2)} \right] + \frac{1}{\lambda}\left(1 - \frac{1}{\lambda_L^2}\right), \tag{30}$$

resulting in an implicit equation in λ_L, which has been solved numerically. For other temperature configurations, a similar derivation can be performed. For a numerical case study, the *Poisson* ratio $\nu = 0.25$ was chosen, which is a commonly applied value for plant tissues. For a given stretch λ, the corresponding lateral stretch λ_L according to (30) is displayed in Figure 5.

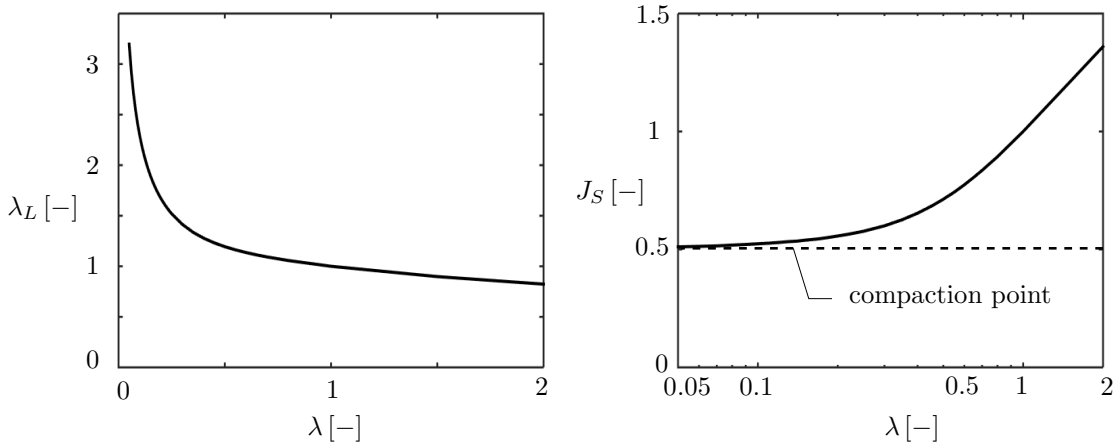

Figure 5: (Left): Lateral stretch - axial stretch for an uniaxial tension-compression test. (Right): Jacobian J_S - axial stretch for an uniaxial tension-compression test. Note that the axis of abscissa is scaled logarithmically. The compaction point is indicated for the compression state.

The sketches in Figure 5 show the lateral stretch λ and the Jacobian J_S as a function of the applied axial stretch, yielding a physically reasonable response. In particular, in the compression regime the volumetric deformation is constraint by the limiting value $\tilde{J}_S$ indicating the point of compaction.

4 CONCLUSION

Within this contribution, the derivation of a material description for frost-resistant plant tissues is addressed. Therefore, a number of basic definitions and considerations are necessary. First, the modelling approach based on the TPM needs to be introduced. Furthermore, the deformation is described in detail under the assumption of thermoelasticity and a kinematic coupling of the ice to the solid skeleton. These notions are crucial for the derivation of the volume fractions of the solids, which essentially determine the compaction point. The compaction point was included in the material description, which has been shown to describe the phenomenon of the compaction point properly.

Acknowledgements. This work has been funded by the German Research Foundation (DFG) as part of the Transregional Collaborative Research Centre (SFB/Transregio) 141 'Biological Design and Integrative Structures'/A01.

REFERENCES

[1] Neuner, G., Xu, B., Hacker, J. Velocity and pattern of ice propagation and deep supercooling in woody stems of *Castanea sativa*, *Morus nigra* and *Querus robur* measured by IDTA. *Tree Physiology* (2010) **30**:1037–1045.

[2] Eurich, L., Schott, R., Wagner, A., Roth-Nebelsick, A., Ehlers, W. Fundamentals of Heat and Mass Transport in Frost-Resistant Plant Tissues. *In Knippers, J. et al. (eds.) Biomimetic Research for Architecture and Building Construction*, Biologically-Inspired Systems, Vol. 9, Springer-Verlag, Cham (2016):97–108.

[3] Pearce, R.S. Plant Freezing and Damage. *Annals of Botany* (2001) **87**:417–424.

[4] Ehlers, W. and Eipper, G. Finite Elastic Deformations in Liquid-Saturated and Empty Porous Solids. *Transport in Porous Media* (1999) **34**:179–191.

[5] Bluhm, J. Constitutive relations for thermo-elastic porous solids. *Zeitschrift für Angewandte Mathematik und Mechanik* (2000) **80**:125–128.

[6] de Boer, R. *Trends in Continuum Mechanics of Porous Media.* Theory and Applications of Transport in Porous Media, Vol. 18, Springer-Verlag, Dordrecht (2005).

[7] Ehlers, W. Foundations of multiphasic and porous materials. *In Ehlers, W. and Bluhm, J. (eds.) Porous Media: Theory, Experiments and Numerical Applications*, Springer-Verlag, Berlin (2002):3–86.

[8] Ehlers, W. Challenges in porous media models in geo- and biomechanical engineering including electro-chemically active polymers and gels. *International Journal of Advances in Engineering Sciences and Applied Mathematics* (2009) **1**:1–24.

[9] Ehlers, W. and Häberle, K. Interfacial Mass Transfer During Gas-Liquid Phase Change in Deformable Porous Media with Heat Transfer. *Transport in Porous Media* (2016) **114**:525–556.

[10] Bluhm, J., Ricken, T., Bloßfeld, M. Ice Formation in Porous Media. *In Markert, B. (ed.) Advances in Extended & Multifield Theories for Continua*, Springer-Verlag, Berlin (2011):153–174.

[11] Eurich, L., Schott, R., Wagner, A., Roth-Nebelsick, A., Ehlers, W. From functional properties of frost-resistant plant tissues towards customised construction materials - A continuum-mechanical approach. *Proceedings in Applied Mathematics and Mechanics* (2016) **16**:81–82.

[12] Hartmann, S. Comparison of the multiplicative decompositions $F = F_\theta F_M$ and $F = F_M F_\theta$ in finite strain thermo-elasticity. *Technical Report Series TU Clausthal* (2012):Fac3-12-01.

[13] Lu, S.C.H. and Pister, K.S. Decomposition of deformation and representation of the free energy function for isotropic thermoelastic solids. *International Journal of Solids and Structures* (1975) **11**:927–934.

[14] Simo, J.C. and Pister, K.S. Remarks on rate constitutive equations for finite deformation problems: computational implications. *Computer Methods in Applied Mechanics and Engineering* (1984) **46**:201–215.

[15] Hartmann, S. The Class of Simo & Pister-type Hyperelasticity Relations. *Technical Report Series TU Clausthal* (2010):Fac3-10-02.

[16] Markert, B. Porous Media Viscoelasticity with Application to Polymeric Foams. *Dissertation Universität Stuttgart, Report No.: II-12* (2005).

[17] Ogden, R.W. Large Deformation Isotropic Elasticity - On the correlation of Theory and Experiment for Compressible Rubberlike Solids. *Proceedings of the Royal Society of London, Series A* (1972) **328**:567–583.

[18] Simo, J.C. and Taylor, R.L. Quasi-incompressible finite elasticity in principal stretches. Continuum basis and numerical algorithms. *Computer Methods in Applied Mechanics and Engineering* (1991) **85**:273–310.